Elevated FTO alleviates sepsis-induced acute kidney injury by regulating macrophage inflammatory phenotypes

XIAONA CHEN[1,2], ZIQI SUN[2,3], JIABO CHEN[2], JINQUAN ZHANG[2,4], ZEYU LIU[2,4], ZHENGZHENG YAN[5], QUAN LI[1-4] and ZHIXIA CHEN[2]

[1]School of Medicine, Southern University of Science and Technology, Shenzhen, Guangdong 518055, P.R. China; [2]Department of Anesthesiology, National Cancer Center/National Clinical Research Center for Cancer/Cancer Hospital and Shenzhen Hospital, Chinese Academy of Medical Sciences and Peking Union Medical College, Shenzhen, Guangdong 518116, P.R. China; [3]Department of Anesthesiology, The First Affiliated Hospital, Jiangxi Medical College, Nanchang University, Nanchang, Jiangxi 330006, P.R. China; [4]Guangzhou University of Chinese Medicine, Guangzhou, Guangdong 510006, P.R. China; [5]Department of Anesthesiology, The Tenth Affiliated Hospital, Southern Medical University (Dongguan People's Hospital), Dongguan, Guangdong 523000, P.R. China

Received June 11, 2025; Accepted October 9, 2025

DOI: 10.3892/ijmm.2025.5689

Abstract. Studies have linked the dysregulation of N6-methyladenosine (m^6A) to sepsis-induced acute kidney injury (SAKI), highlighting the persistent challenge of managing excessive proinflammatory cytokine production and subsequent organ dysfunction. The present study, by analyzing the GSE32707 and GSE69063 datasets, found that fat mass and obesity-associated protein (FTO) was the sole m^6A-related gene markedly downregulated in the peripheral blood transcriptome of patients with sepsis. It further demonstrated that septic mice subjected to cecal ligation and puncture presented increased m^6A modifications and reduced FTO expression in both renal tissues and peritoneal macrophages. The findings revealed that increased levels of FTO was associated with reduced mortality and kidney damage during sepsis and that the upregulation of FTO in lipopolysaccharide-stimulated macrophages led to decreased production of proinflammatory cytokines. Mechanistically, through multiomic analysis of macrophages, the present study identified a novel mechanism involving matrix metalloproteinase 9 (MMP-9) as a direct target of FTO, which positively affects its translation efficacy. Furthermore, both *in vivo* and *in vitro* data confirmed that reduced MMP-9 levels exerted adverse effects on mitigating inflammatory responses and alleviating renal injury. Overall, the findings underscored the critical role of the FTO/m^6A/MMP-9 axis in the regulation of proinflammatory secretion and improved our understanding of the transcriptomic landscape during the progression of SAKI, suggesting that targeting the FTO/m^6A/MMP-9 axis may offer therapeutic potential for mitigating renal injury in septic patients.

Correspondence to: Professor Zhixia Chen, Department of Anesthesiology, National Cancer Center/National Clinical Research Center for Cancer/Cancer Hospital and Shenzhen Hospital, Chinese Academy of Medical Sciences and Peking Union Medical College, 113 Baohe Road, Longgang, Shenzhen, Guangdong 518116, P.R. China
E-mail: chenzhixia2007@163.com

Professor Quan Li, School of Medicine, Southern University of Science and Technology, 1088 Xueyuan Avenue, Nanshan, Shenzhen, Guangdong 518055, P.R. China
E-mail: quanligene@126.com

Abbreviations: m^6A, N6-methyladenosine; SAKI, sepsis-induced acute kidney injury; CLP, cecal ligation and puncture; FTO, fat mass and obesity-associated protein; LPS, lipopolysaccharide; IL-6, interleukin-6; TNF-α, tumor necrosis factor-α; MMP-9, matrix metalloproteinase 9; ALI, acute lung injury; GEO, gene expression omnibus; DEGs, differentially expressed genes; FC, fold change; qPCR, quantitative PCR; DMEM, Dulbecco's modified Eagle's medium; FBS, fetal bovine serum; IHC, immunohistochemistry; H&E, hematoxylin and eosin staining; AAV, adeno-associated virus; RNA-seq, transcriptome sequencing; MeRIP-seq, methylated RNA immunoprecipitation sequencing; GO, gene ontology; CHX, cycloheximide; Co-IP, Co-immunoprecipitation; RT, Room temperature

Key words: sepsis-induced acute kidney injury, N6-methyladenosine, fat mass and obesity-associated protein, matrix metalloproteinase 9

Introduction

Sepsis is a prevalent inflammatory response induced by microbial infection, with severe manifestations potentially leading to multiorgan dysfunction (1). The current literature indicates that the incidence of sepsis-induced acute kidney injury (SAKI) among patients with sepsis in intensive care units is ~51%, with a mortality rate of 41%. Despite these statistics, effective therapeutic interventions remain limited (2). Studies have revealed that the pathogenesis of SAKI involves multiple mechanisms, particularly inflammation, which activates innate

immune components such as monocytes-macrophages, natural killer T cells and neutrophils, all of which are integral to the injury response in SAKI (3,4). Positive outcomes correlate with reduced levels of inflammatory factors, such as interleukin-6 (IL-6) and tumor necrosis factor-α (TNF-α), indicating that early inflammatory response suppression benefits patients with high-risk SAKI (5).

As essential components of the innate immune system, macrophages play a critical role in regulating inflammatory responses when activated. Studies have reported that renal macrophages are involved in regulating kidney infections, ischemia-reperfusion injury, drug toxicity, and diabetic nephropathy (6-8). In SAKI, infiltration of glomerular and interstitial macrophages is observed, with proinflammatory macrophages predominating in the early stages; these macrophages stimulate leukocyte infiltration and proinflammatory cytokine secretion and produce cytotoxic substances. However, the transition from the M1 phenotype to the M2 phenotype signifies a shift from the injury phase to the repair phase in the ischemically damaged kidney and is essential for tubular cell proliferation and functional recovery (9). In addition, this phenotypic conversion can lead to the secretion of anti-inflammatory cytokines and matrix metalloproteinases (MMPs), which mediate the cleavage of chemokines and chemotactic agents, inhibit inflammatory cell activity and aid in kidney injury repair (10). Moreover, dysregulation of the macrophage phenotypic transition causes prolonged inflammation and impairs tissue healing (11). Thus, in-depth research on the mechanisms of macrophages in sepsis is crucial for the development of new therapeutic strategies to mitigate SAKI.

The remarkable plasticity of macrophages to modify their phenotypes and functions in response to environmental stimuli is crucial for maintaining health and combating disease. However, the molecular mechanisms underlying this remarkable plasticity remain only partially understood. Advances in the field of epigenetics have illuminated the complex regulatory networks that govern macrophage behavior by affecting mRNA stability, folding, degradation, splicing, translation, and export (12). Epigenetics involves the differential expression of genes resulting from modifications in noncoding sequences, which can influence gene expression patterns in response to environmental stimuli, thereby affecting cellular function and organ homeostasis and contributing to processes such as inflammation, tissue repair and immune regulation (13). N6-methyladenosine (m^{6}A) is a predominant posttranscriptional modification in eukaryotic RNAs (14,15).

m^{6}A methylation is catalyzed primarily by m^{6}A 'writer' enzymes [such as [Wilms' tumor 1-associating protein (WTAP), methyltransferase-like 3 (METTL3), vir like m^{6}A methyltransferase associated (VIRMA), methyltransferase-like 14 (METTL14) and RNA binding motif protein 15 (RBM15), which catalyze methylation reactions), 'eraser' enzymes [such as fat mass and obesity-associated protein (FTO)] and ALKBH5, which remove m^{6}A modifications and regulate RNA stability) and 'reader' enzymes [such as YTH domain family proteins 1-3 (YTHDF1-3), YTH domain-containing proteins 1-2 (YTHDC1-2), and Insulin-like growth factor-2 mRNA-binding proteins (IGF2BPs), which recognize m^{6}A-modified RNA] (16). Dysregulation of these enzymes can markedly affect macrophage behavior. For example, the upregulation of IGF2BP1 in SAKI is linked to renal dysfunction and damage through the enhancement of macrophage migration inhibitory factor-related pyroptosis via the activation of the NLR family pyrin domain containing 3 (NLRP3) inflammasome (17). Similarly, FTO downregulates acyl-CoA synthetase long-chain family member in an m^{6}A-dependent manner to inhibit ferroptosis and alleviate macrophage inflammation (18). In acute lung injury (ALI), elevated METTL14 and increased m^{6}A levels are detected in circulating monocyte-derived macrophages, which are recruited to and infiltrate the lungs, suggesting that METTL14-induced NLRP3 inflammasome activation exacerbates ALI (19). These findings underscore the potential of m^{6}A methylation as a critical mediator of cellular injury and disease pathogenesis. An analysis of the datasets GSE32707 (20) and GSE69063 (21) revealed that FTO was the only gene among the m^{6}A-associated proteins that exhibited simultaneous and significant downregulation in the transcriptome of peripheral blood samples from patients with sepsis. Nevertheless, few studies have explored the precise role of FTO in regulating macrophage reprogramming in SAKI.

Thus, in the present study, the regulatory mechanisms of m^{6}A methylation in macrophages during SAKI were investigated. The overexpression of FTO in SAKI mitigated renal damage and reduced the expression and production of proinflammatory cytokines by modulating the m^{6}A modification of MMP-9 mRNA. Conversely, knocking down MMP-9 exacerbated renal dysfunction and renal damage and promoted the production of proinflammatory factors both *in vivo* and *in vitro*. Therefore, it was hypothesized that targeting FTO could be a promising alternative therapeutic strategy for the treatment of SAKI in the future.

Materials and methods

Bioinformatic methods. The sepsis-related single-cell RNA sequencing (scRNA-seq) dataset GSE32707 and sepsis-related RNA sequencing dataset GSE69063, pertaining to peripheral blood mononuclear cells from patients, were obtained from the Gene Expression Omnibus (GEO) database (https://www.ncbi.nlm.nih.gov/geo/). The 'limma' package in R (https://bioconductor.org/packages/limma/; version3.58.1) was used to identify differentially expressed genes (DEGs) linked to sepsis. Genes were identified based on an adjusted P-value <0.05 and an absolute $\log_2$-fold change (FC) >1.

Mice. A total of 125 male C57BL/6 mice (~25g; aged 6-8 weeks) were supplied by SPF (Beijing) Biotechnology Co., Ltd. and used for all the experimental procedures. Each mouse was kept in a ventilated cage in a pathogen-free environment (temperature, 20-26˚C; humidity, 40-70%; under a 12-h light/dark cycle) and was provided with a standard rodent diet. All experimental procedures involving the care and use of mice were approved by the Ethics Committee of Dongguan People's Hospital (approval no. IACUC-AWEC-202406500R1). The mice underwent moderate cecal ligation and puncture (CLP) surgery and their survival rates were subsequently monitored. Blood and tissue samples were collected at 12 or 24 h after surgery.

CRISPR/Cas9-regulated knockout of MMP-9. A total of 6 male *Mmp9*$^{-/-}$ mice (6-8 weeks old) were used in the present study. Mice were housed in a facility with 12-h light/dark cycle at 23±3˚C and 40-70% humidity. To generate the MMP-9 knockout mice used in the present study, the one-step CRISPR-Cas9 zygote-injection protocol that has been extensively validated in the literature was followed (22). Briefly, the single-guide (sg)RNA sequences used to target the MMP-9 gene (gRNA-A1, 5'-CCATGACGATCTCAC AGCTCGGG-3'; gRNA-A2, 5'-CAGGCTCTCTACTGG GCGTTAGG-3'; gRNA-B1, 5'-GTTCACGAGACCTCA GTTGATGG-3'; and gRNA-B2, 5'-ATTCAGTTGCCCCTA CTGGAAGG-3') were designed and synthesized by Cyagen Biosciences, Inc. Fertilized eggs (n=100) were generated by *in vitro* fertilization: oocytes were harvested from 5 female C57BL/6JCya and sperm obtained from 2 male C57BL/6JCya (all mice supplied from Cyagen Biosciences, Inc.). Then mixed sgRNA/Cas9 protein complexes were subsequently assembled immediately before injection by combining Cas9 protein and the four sgRNAs and co-injected into fertilized eggs. The injected embryos were cultured in KSOM medium overnight and those developed to the two-cell stage were transferred into the oviduct of pseudopregnant ICR female mice. The F0 founder mice were identified by PCR, which were bred to wild type C57BL/6JCya mice to test germ line transmission and F1 animal generation. The F1 mice were screened by PCR amplification by using the following wild-type (WT) primers: F1, 5'-CCAGTGAGAAGCATC TAAGAGAAG-3'; R1, 5'-GACTCCTTGGGGAAGGAA AGATG-3'; *Mmp9*$^{-/-}$ primers: F2, 5'-CCAGTGAGAAGC ATCTAAGAGAAG-3'; R2, 5'-GACACAGTCTGACCTGAA CCATAA-3'. Homozygous *MMP9*$^{-/-}$ mice were obtained by inter-crossing heterozygotes and were verified by PCR and western blotting. All animal studies were performed in accordance with the guidelines approved by the Animal Experimentation Ethics Committee of Cyagen Biosciences, Inc. (approval no. GACU23-MS004-788).

Cell culture. The RAW264.7 cell line (cat. no. CL-0190; Procell Life Science & Technology Co., Ltd.) was cultured in Dulbecco's modified Eagle's medium (DMEM; cat. no. C11995500BT; Gibco; Thermo Fisher Scientific, Inc.) supplemented with 10% fetal bovine serum (FBS; cat. no. FND500; Shanghai ExCell Biology, Inc.). Mycoplasma testing was performed on the cell lines with a MycoBlue Mycoplasma Detector kit (cat. no. D101; Vazyme Biotech Co., Ltd.). After stimulation with 1 μg/ml LPS (cat. no. L2630; MilliporeSigma), at various time points, the supernatant, mRNA, and proteins were collected for subsequent analysis.

Lentiviral constructs. For RNA interference (RNAi) mediated by lentiviruses, short hairpin (sh)RNA targeting MMP-9 was generated by Shanghai GeneChem Co., Ltd. All lentiviral particles were generated with a 2nd packaging system. 293T cells (cat. no. GNHu44; Cell Bank, Chinese Academy of Sciences) were seeded at 5x10^6 cells per 10-cm dish 24 h before transfection. For one dish, a total of 45 μg plasmid DNA [transfer (GV):packaging (pHelper 1.0):envelope (pHelper 2.0)=4:3:2] was transfected with transfection kit (cat. no. GRCT105; Shanghai GeneChem Co., Ltd.). Medium was replaced 8-12 h post-transfection; viral supernatants were harvested at 48 h, filtered (0.45 μm, cat. no. SLHP033R; Millipore) and centrifuged at 75,000 x g for 2 h at 4˚C. The pelleted virions were gently resuspended in ice-cold PBS, vortexed briefly, and centrifuged again at 10,000 x g for 5 min at 4˚C to remove debris. The final concentrated lentivirus was aliquoted and stored at -80˚C until use. The sequences of the shRNAs used were as follows: 5'-CACTTA CTATGGAAACTCAAA-3' and 5'-GACCATCATAACATC ACATAC-3'. A lentivirus that overexpresses mouse FTO and insulin-like growth factor 2 mRNA-binding protein 3 (IGF2BP3) was also created by Shanghai GeneChem Co., Ltd. RAW264.7 cells were transfected with these recombinant lentiviral plasmids to establish the FTO-overexpressing (oe-FTO) RAW264.7 cell line and the MMP-9-knockdown (shMMP-9) RAW264.7 cell line at the appropriate multiplicity of infection (MOI=30); an empty lentiviral vector was used as a control for transfection. At 72 h post-transduction cells were selected with puromycin (5 μg/ml; cat. no. A1113803; Gibco; Thermo Fisher Scientific, Inc.) for 7 days, then maintained in 2 μg/ml puromycin until assays were performed. All experiments were carried out between passage 3 and 6 after selection.

CLP. The CLP surgery was performed according to the established protocol by Rittirsch *et al* (23) and Liu *et al* (24), with minor adaptations. Briefly, mice were anesthetized by induction started with 4% sevoflurane in an acrylic chamber and the concentration was adjusted accordingly by the absence of pedal withdrawal reflex. Maintenance anesthesia was administered at 2-2.5% sevoflurane via a nose cone, with continuous monitoring of anesthetic depth throughout the procedure. Following abdominal shaving and aseptic preparation, a 1.5-2 cm midline laparotomy was performed to exteriorize the cecum. The cecum was ligated at ~50% between the cecal tip and the ileo-cecal valve with 5-0 silk suture and punctured with a 21-gauge needle. A small droplet of feces was extruded to ensure patency before the cecum was returned to the abdominal cavity. The incision was closed in two layers with 5-0 silk. Postoperatively, mice received 1 ml pre-warmed (37˚C) sterile saline subcutaneously, along with buprenorphine (0.05 mg/kg, s.c.) administered every 8 h. Food and water were provided *ad libitum*.

Adeno-associated virus (AAV). The eight-week-old C57BL/6J male mice received tail vein injections of Ctrl-AAV or FTO-AAV (Shanghai GeneChem Co., Ltd.), with each mouse receiving 10^{11} viral particles. The enhanced green fluorescent protein (EGFP) gene was carried by the AAV. Gene overexpression was verified in mice injected with AAVs by western blotting and immunofluorescence (IF) one month later.

Isolation of peritoneal macrophages (PMs). Peritoneal lavage fluid was collected and centrifuged at 300 x g for 10 min at 4˚C, after which the red blood cells were lysed by Red Blood Cell Lysis Buffer (cat. no. R1010; Beijing Solarbio Science & Technology Co., Ltd.). F4/80+ PMs were subsequently isolated using a kit (cat. no. 100-0659; Stemcell Technologies, Inc.) and cultured in DMEM supplemented with 5% FBS and 100 IU/ml penicillin-streptomycin before use.

Dot blot assay. Total RNA (2 μg/μl) was heated to 95˚C for 5 min, and 2 μl of mRNA was spotted onto an Amersham Hybond-N+ membrane (cat. no. RPN303B; Cytiva). The membrane was crosslinked, blocked for 1 h at room temperature (RT) with 5% non-fat dry milk (cat. no. 36120ES76; Shanghai Yeasen Biotechnology Co., Ltd.), incubated with an anti-m^{6}A antibody (cat. no. ab284130; Abcam) overnight at 4˚C. The following day, after incubation with an HRP-conjugated secondary antibody, Goat Anti-Rabbit IgG(H+L) (peroxidase/HRP conjugated; 1:8,000; cat. no. E-AB-1003; Wuhan Elabscience Biotechnology Co., Ltd.), for 1 h at RT, the membrane were detected with ECL A/B reagents (cat. no. 1705061; Bio-Rad Laboratories, Inc.) and visualized on a ChemiDoc system (G:B0XChemiXX9; Syngene).

In vitro phagocytosis assay. The RAW 264.7 cells were incubated with pHrodo Green *E. coli* BioParticles (cat. no. P35366; Invitrogen; Thermo Fisher Scientific, Inc.) at 37˚C for 1 h and then fixed and stained with rhodamine phalloidin (PHDR1; Cytoskeleton, Inc.) at 4˚C for 30 min. The phagocytosis efficiency was evaluated as the MFI of the internalized pHrodo Green bioparticles per macrophage.

Pretreatment with recombinant MMP-9 (rMMP9). Cells were pretreated with recombinant MMP-9 protein (cat. no. 50560-MNAH1; Sino Biological) at a concentration of 100 ng/ml for 2 h at 37˚C. The cells were subsequently stimulated with LPS (1 μg/ml) for an additional 6 h.

Immunofluorescence (IF) staining. For sectioning, the samples were fixed in 4% paraformaldehyde (cat. no. BL539A; Biosharp Life Sciences) for 24 h at RT, washed three times (5 min each) with phosphate-buffered saline (PBS; cat. no. C0221A; Beyotime Biotechnology), dehydrated through a graded ethanol series, cleared in xylene (cat. no. X821391; Shanghai Macklin Biochemical Co., Ltd.), .and embedded in paraffin. The cells were permeabilized with a 0.1-0.5% Triton X-100 solution and blocked with 5% normal goat serum (cat. no. C0265; Beyotime Biotechnology) in PBS for 1 h at 4˚C. Following permeabilization, the sections or cells were incubated with the corresponding antibodies (1;100) overnight at 4˚C and a secondary antibody (1:500; cat. no. A0423; Beyotime Biotechnology) for 1 h at RT. Following DAPI staining (1-2 drops; cat. no. P0131; Beyotime Biotechnology) for 5 min at RT, fluorescence images were acquired using a confocal fluorescence microscope at multiple magnifications: x10, x20, or x63. For cells, the IF staining steps were the same as aforementioned.

Immunohistochemistry (IHC) and histological analysis. Tissues were fixed in 4% paraformaldehyde (cat. no. BL539A; Biosharp Life Sciences) for 24 h at RT, followed by dehydration with various ethanol concentrations and, finally, the samples were embedded in paraffin for sectioning. Using a microtome, the samples were sliced into 5 μm sections and then deparaffinized and hydrated. Antigen retrieval was performed by heating slides in 10 mM sodium citrate buffer (cat. no. BL604A, Biosharp Life Sciences) for 10-15 min at 95˚C, followed by cooling to RT. Then an appropriate volume (1-2 drops) of endogenous peroxidase blocking reagent (cat. no. PV-6000D; Beijing Zhongshan Jinqiao Biotechnology Co., Ltd.) was applied, and the sections were incubated for 10 min at RT. Primary antibodies diluted in antibody diluent (cat. no. ZLI-9029, Beijing Zhongshan Jinqiao Biotechnology Co., Ltd.) were applied overnight at 4˚C. The following antibodies were used: anti-MMP-9 (1:100; cat. no. ab228402; Abcam), anti-FTO (1:200; cat. no. ab126605; Abcam), anti-CD86 (1:100; cat. no. 19589; Cell Signaling Technology, Inc.), anti-CD163 (1:100; cat. no. GB113751; Wuhan Servicebio Technology Co., Ltd.) and anti-F4/80 (1:200; cat. no. GB12027; Wuhan Servicebio Technology Co., Ltd.). After three PBS washes, sections were incubated with HRP-conjugated goat anti-rabbit or anti-rat secondary antibody (1-2 drops; cat. no. PV-6000D; Beijing Zhongshan Jinqiao Biotechnology Co., Ltd.) for 30 min at 37˚C. Immunoreactivity was developed with DAB substrate kit (100 μl; cat. no. PV-6000D; Beijing Zhongshan Jinqiao Biotechnology Co., Ltd.). Nuclei were counterstained with hematoxylin (cat. no. C0107; Beyotime Biotechnology) for 3-5 min at RT, followed by blueing in distilled water. Slides were dehydrated, cleared and mounted with neutral balsam. After staining, the samples were analyzed using a light microscope, and the images were independently evaluated by two pathologists. The semiquantitative immunoreactivity score was calculated in a blinded manner.

Hematoxylin and eosin (H&E) staining. H&E staining was performed to observe tissue morphological changes, and the histological scores for kidney injury were assessed (25). The severity of kidney tissue damage was evaluated based on luminal cell swelling, renal interstitial congestion, cell death, edema and protein casts. Kidney injury was scored on a 5-point scale: 0 for normal structure, 1 for ≤10% damage, 2 for 11-25% damage, 3 for 26-45% damage, 4 for 46-75% damage, and 5 for ≥76% damage (26).

Reverse transcription-quantitative (RT-q) PCR. Total RNA was extracted from the tissues or cells using TRIzol® reagent (cat. no. 15596026; Invitrogen; Thermo Fisher Scientific, Inc.) according to the manufacturer's protocol and then 1 μg of total RNA was reverse-transcribed into cDNA with a PrimeScript RT Reagent Kit (cat. no. 11141ES60; Shanghai Yeasen Biotechnology Co., Ltd.) according to the manufacturer's protocol. qPCR was subsequently performed using cDNA templates, primers and SYBR Green Mix (cat. no. 11184ES08; Shanghai Yeasen Biotechnology Co., Ltd.) according to the manufacturer's protocol. Thermocycling conditions: 95˚C for 2 min, followed by 40 cycles of 95˚C for 10 sec and 60˚C for 30 sec. A melting-curve analysis (65-95˚C, 0.5˚C increments) was included to confirm product specificity. GAPDH or β-actin served as internal controls for coding genes. The calculations were based on the $2^{-\Delta\Delta Cq}$ method (27) and the sequences of the primers used are listed in Table I.

Western blotting. Total protein was extracted using RIPA lysis buffer (cat. no. WB3100; Suzhou NCM Biotech Co., Ltd.) with a protease inhibitor cocktail (cat. no. HY-K0010; MedChemExpress). Protein concentration was determined with the BCA protein assay kit (cat. no. P0009; Beyotime Biotechnology). Protein (~30 μg per lane) was separated on 8-12% SDS-polyacrylamide gels according to the molecular weight of the target proteins and electro-transferred onto

Table I. Primers for reverse transcription-quantitative PCR (murine).

Gene	Forward primer (5'-3')	Reverse primer (5'-3')
FTO	TTCATGCTGGATGACCTCAATG	GCCAACTGACAGCGTTCTAAG
ALKBH5	GCATACGGCCTCAGGACATTA	TTCCAATCGCGGTGCATCTAA
METTL3	CCCAACCTTCCGTAGTGATAG	TGGCGTAGAGATGGCAAGAC
METTL14	GGTCGGAGTGTGAACCTGAT	GGTCCTCTTCCACGCTGTAT
WTAP	TAATGGCGAAGTGTCGAATG	CTGCTGTCGTGTCTCCTTCA
MMP-9	GCAGAGGCATACTTGTACCG	TGATGTTATGATGGTCCCACTTG
IL-6	TAGTCCTTCCTACCCCAATTTCC	TTGGTCCTTAGCCACTCCTTC
TNF-α	CAGGCGGTGCCTATGTCTC	CGATCACCCCGAAGTTCAGTAG
GAPDH	AGGTCGGTGTGAACGGATTTG	GGGGTCGTTGATGGCAACA

0.22 μm polyvinylidene difluoride (PVDF) membranes (cat. no. ISEQ00010; MilliporeSigma). Then membranes were blocked for 1 h at RT with 5% non-fat dry milk (cat. no. 36120ES76; Shanghai Yeasen Biotechnology Co., Ltd.). Primary antibodies were diluted in primary antibody dilution buffer (cat. no. P0023A; Beyotime Biotechnology) and incubated overnight at 4˚C. The following antibodies were used: anti-β-tubulin (cat. no. 30302ES60; Shanghai Yeasen Biotechnology Co., Ltd.), anti-β-actin (cat. no. 3700; Cell Signaling Technology, Inc.), anti-GAPDH (cat. no. 30201ES60; Shanghai Yeasen Biotechnology Co., Ltd.), anti-MMP-9 (cat. no. ab228402; Abcam), anti-FTO (cat. no. ab126605; Abcam), anti-CD206 (cat. no. 24595; Cell Signaling Technology, Inc.), anti-CD86 (cat. no. 19589; Cell Signaling Technology, Inc.), anti-NF-κB (cat. no. 8242; Cell Signaling Technology, Inc.), anti-IGF2BP3 (cat. no. 14642-1-AP; Proteintech Group, Inc.) and anti-phosphorylated NF-κB (cat. no. 3033; Cell Signaling Technology, Inc.). The following day, after incubation with an HRP-conjugated secondary antibody (1:8,000; cat. no. E-AB-1003 and cat. no. E-AB-1001; Wuhan Elabscience Biotechnology Co., Ltd.) for 1 h at RT, the proteins in the membrane were detected with ECL A/B reagents (cat. no. 1705061; Bio-Rad Laboratories, Inc.) and imaged on a ChemiDoc system (G:B0XChemiXX9; Syngene).

Co-immunoprecipitation (Co-IP). RAW264.7 cells ($5x10^6$ per 10-cm dish) were collected and lysed in 1 ml IP lysis buffer (cat. no. P0013; Beyotime Biotechnology) with protease inhibitors (cat. no. HY-K0010; MedChemExpress) for 30 min. Lysates were centrifuged at 4˚C and 12,000 x g for 10 min. Then they were divided into input, anti-IgG and anti-IGF2BP3 groups. Protein A/G magnetic beads (cat. no. HY-K0202; MedChemExpress; 25 μl per reaction) were preincubated with anti-IGF2BP3 (cat. no. 14642-1-AP; Proteintech Group, Inc.) or anti-IgG (cat. no. 2729S; Cell Signaling Technology, Inc.) antibodies at 4˚C for 2 h, which then were added to 400 μl lysates and incubated at 4˚C overnight. The tubes were placed on the DynaMag™-2 magnet (cat. no. 12321D; Invitrogen; Thermo Fisher Scientific, Inc.) for 1 min on ice and the magnetic-bead washing was performed. Following three washes with buffer consisting of 1X PBS containing 0.5% Tween-20 (cat. no. ST1727; Beyotime Biotechnology), the coprecipitated proteins were eluted by boiling in 1X SDS sample buffer (95˚C; 10 min) and subjected to analysis through western blot.

Puromycin labeling. The cells at 70% confluence were treated with 50 μg/ml puromycin for 10 min at 37˚C. The cells were lysed and processed for western blot analysis. The lysates were incubated with a puromycin-specific antibody (cat. no. PMY-2A4; 0.5 μg/ml; Developmental Studies Hybridoma Bank), followed by incubation with a secondary antibody. Finally, the protein bands were visualized to assess puromycin incorporation.

RNA stability. To assess MMP-9 mRNA stability, cells were treated with actinomycin D (5 μg/ml; cat. no. M4881Abmole Bioscience, Inc.) to inhibit transcription. Samples were collected at 0, 2, 4, 6, 8 and 10 h posttreatment. Total RNA was subsequently extracted, and the expression of MMP-9 mRNA was assessed through RT-qPCR.

Protein decay assay. After pretreatment with LPS (1 μg/ml) for 12 h, the macrophages were exposed to medium supplemented with cycloheximide (CHX; 50 μg/ml) for various durations before western blot analysis was performed.

Enzyme-linked immunosorbent assay (ELISA). The release of IL-6 and TNF-α was measured using specific ELISA kits (cat. nos. M6000B and MTA00B; R&D Systems). Serum levels of creatinine (Cr; cat. no. C013-2-1; Nanjing Jiancheng Bioengineering Institute) and blood urea nitrogen (BUN; cat. no. C011-2-1; Nanjing Jiancheng Bioengineering Institute) were evaluated according to the kit manufacturers' instructions.

Cell Counting Kit-8 (CCK-8) and lactate dehydrogenase (LDH) assays. Cell viability was assessed using a CCK-8 assay (cat. no. CA1210; Beijing Solarbio Science & Technology Co., Ltd.), and LDH levels in the cell culture supernatant were measured using an LDH assay kit (cat. no. C20300; Thermo Fisher Scientific, Inc.).

Methylated RNA immunoprecipitation sequencing (MeRIP-seq) and MeRIP-qPCR. Poly(A) RNA was initially isolated, and 3 μg of RNA was retained as an input group. PGM beads were incubated with 2 μl of anti-m^6A or anti-rabbit

immunoglobulin G (IgG) antibodies, which were subsequently combined with RNA. The methylated mRNAs were subsequently purified and further quantified through qPCR, with m^{6}A enrichment in each sample normalized to the input.

MeRIP-seq and RNA-seq data deposition. MeRIP-seq and RNA-seq raw reads and processed count matrices have been uploaded to the NCBI Gene Expression Omnibus (GEO) under accession numbers: GSE297677 (https://www.ncbi.nlm.nih.gov/geo/query/acc.cgi?acc=GSE297677) and GSE297679 (https://www.ncbi.nlm.nih.gov/geo/query/acc.cgi?acc=GSE297679).

Quantitative analysis of western and dot blots. After ECL exposure, chemiluminescent signals were captured. Non-saturated 8-bit TIFF files were analyzed with ImageJ v. 1.51j8 (National Institutes of Health) (28). For western blots, each lane was outlined with the rectangular selection tool, background subtracted with the 'rolling-ball' radius set to 50 pixels, and band intensities calculated as the area under the peak. Values were normalized to the corresponding β-actin or GAPDH signal and expressed as fold-change relative to the sham/control lane loaded on the same gel. Dot-blot arrays were processed similarly: Global m^{6}A levels were calculated as the ratio of m^{6}A dot intensity to total RNA (methylene-blue) signal. All data were exported to perform statistical analysis.

Statistical analysis. The results are shown as the mean±standard deviation and statistical tests were performed with GraphPad Prism software (Dotmatics, version 8.0.1). Survival curves were compared between experimental and control groups using the log-rank test; due to the limited sample size, hazard ratios were not computed. The data were analyzed with one-way ANOVA and Tukey's post hoc test for comparing multiple groups or an unpaired two-tailed Student's t-test for comparing two groups. For the time-course data, observations at different time points are independent rather than repeated measures, and a one-way ANOVA was therefore used instead of repeated-measures ANOVA. $P<0.05$ was considered to indicate a statistically significant difference.

Results

SAKI is accompanied by increased m^{6}A methylation and reduced FTO expression. Studies have demonstrated a close association between epigenetic mechanisms and sepsis; however, the specific relationship between m^{6}A methylation levels and sepsis remains inadequately understood (29,30). The screening process is illustrated in Fig. 1A. As depicted, differential expression analyses were conducted utilizing the limma package, resulting in the identification of 13 genes associated with m^{6}A modification, which are represented in a scatter plot (Fig. 1B). In particular, FTO was identified as the only gene whose expression was markedly downregulated, as shown by analysis of the GSE32707 dataset from the Gene Expression Omnibus database. To explore this finding further, the present study analyzed the GSE69063 dataset and demonstrated a decrease in the expression of FTO among m^{6}A-related proteins within the transcriptome of peripheral blood samples from patients with sepsis (Fig. 1C).

Furthermore, a septic mouse model was established by performing CLP surgery to simulate clinical polymicrobial sepsis. Histological analysis revealed that the CLP-treated mice exhibited inflammatory infiltration across various organs (Fig. S1A). IL-6 secretion rapidly increased within 12 h following CLP (Fig. S1B). IHC and Western blot analyses revealed that FTO expression was lower in the kidney tissues of CLP-induced septic mice than in the kidney tissues of sham-operated mice (Figs. 1D and E and S1C and D). Consistent with the decrease in FTO expression, the results of the dot blot array revealed a notable increase in m^{6}A modification levels in the kidney tissues of septic mice (Figs. 1F and S1E). Taken together, these findings suggested the potential involvement of FTO in SAKI.

Overexpression of FTO inhibits the proinflammatory response of macrophages. As previously reported, macrophage polarization represents a promising novel therapeutic approach for facilitating repair in AKI (31). To investigate the alterations in FTO expression in macrophages from septic mice, PMs were isolated from these mice. Western blot and qPCR analyses revealed a decrease in FTO expression in the PMs of septic mice compared with those of sham-operated mice (Fig. 2A and B). Additionally, blotting assays revealed a concomitant increase in m^{6}A methylation levels in macrophages treated with 1 μg/ml LPS for 0, 6 and 12 h (Figs. 2C and S1F). LPS-treated macrophages were then collected for qPCR analysis to assess the mRNA expression levels of enzymes related to m^{6}A modification. The findings indicated that among the key m^{6}A-related enzymes, both ALKBH5 and FTO were downregulated, which is consistent with the observed m^{6}A modification trends; FTO demonstrated the most pronounced decrease in expression (Figs. 2D and S1G and H). Western blotting and qPCR revealed significant, time-dependent downregulation of FTO expression in LPS-treated macrophages (Fig. 2E and F). These results suggested that FTO is a crucial protease involved in m^{6}A modification and plays a pivotal role in the reprogramming of macrophages during sepsis.

To investigate the regulatory function of FTO in macrophages, macrophages overexpressing FTO were generated by transfecting them with lentiviral vectors encoding mouse FTO inserts according to the endogenous expression of FTO. The efficacy of the transfection was confirmed by western blotting (Figs. 2G and S1I). Next, CCK-8 and LDH assays were performed and it was found that the overexpression of FTO in macrophages neither induced cytotoxic effects nor influenced macrophage proliferation (Fig. 2H and I). Given that phagocytosis is the principal mechanism through which macrophages eradicate pathogens, phagocytosis assays were performed. The results demonstrated that FTO upregulation did not alter the phagocytic capacity of macrophages compared with that of the control group (Fig. 2J and K). Macrophages secrete proinflammatory cytokines that exacerbate SAKI by promoting renal tubular epithelial cell injury and impairing mitochondrial function (32). Surprisingly, ELISAs revealed that the secretion of the inflammatory factors IL-6 and TNF-α in the supernatant of LPS-stimulated macrophages was markedly inhibited by FTO upregulation (Fig. 2L). These observations were corroborated by qPCR experiments (Fig. 2M). Moreover, examination of classic pathways associated with

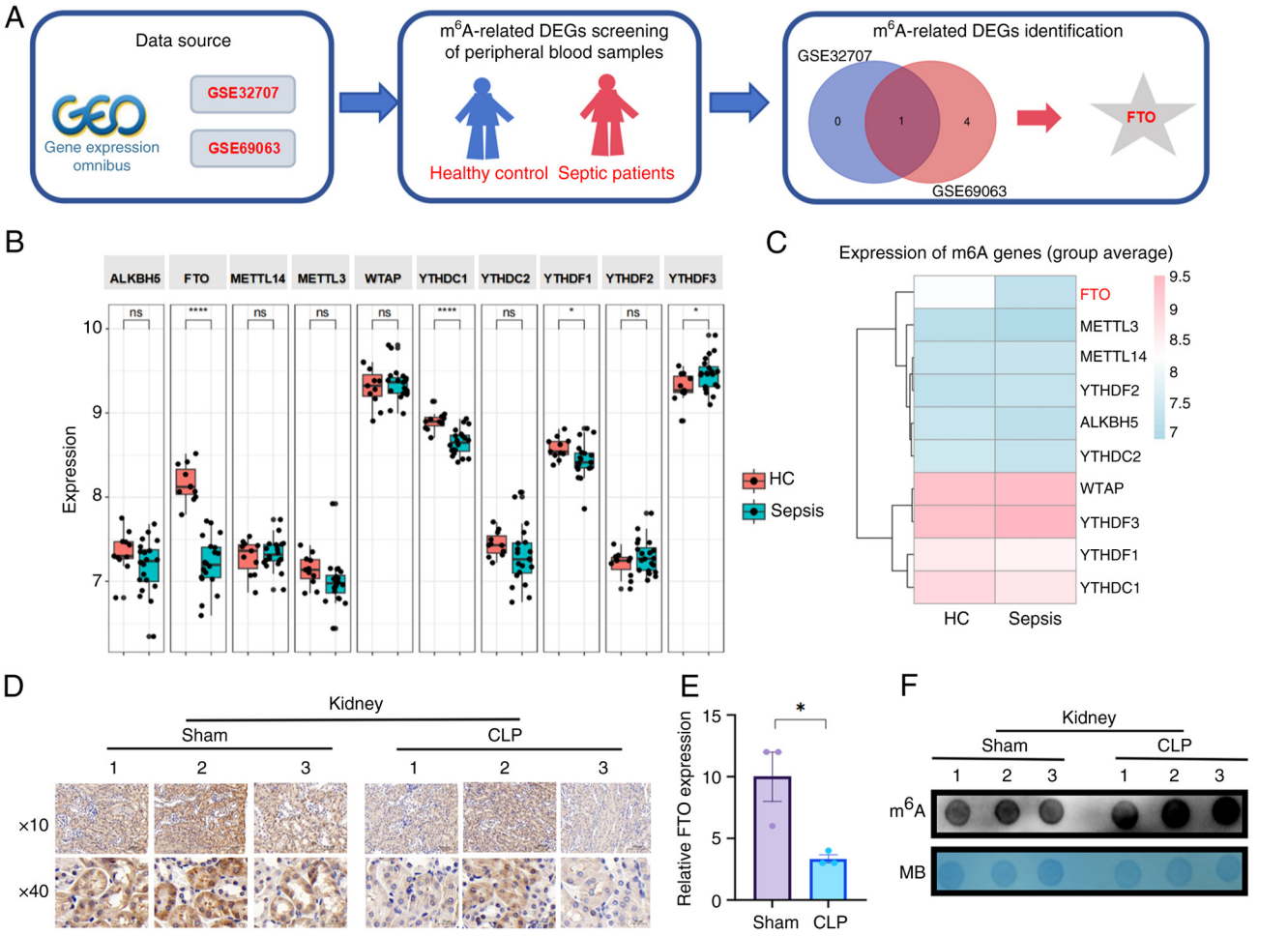

Figure 1 FTO expression is downregulated and m^{6}A methylation increased in SAKI. (A) Schematic illustration of the screening process employed to identify key genes associated with m^{6}A modification in sepsis. (B) Scatter plot depicting the differential expression of m^{6}A-related genes, highlighting FTO as the only gene whose expression was markedly downregulated in the sepsis group (Sepsis) compared with that in the NC goup in the GSE32707 dataset. (C) Analysis of the GSE69063 dataset revealed decreased FTO expression in the transcriptomes of m^{6}A-related proteins in peripheral blood samples from patients with sepsis (Sepsis) compared with those from HCs. (D) Representative IHC staining and (E) quantification of FTO expression in kidney tissues from CLP-induced septic mice compared with those from sham-operated controls (n=3; P<0.05). (F) Dot blot analysis revealed a significant increase in the global m^{6}A modification level in the kidney tissues of CLP-induced septic mice (n=3; P<0.05). All the data are presented as the mean±standard error of the mean. Data (in D and F) were analyzed using an unpaired two-tailed Student's t-test. *P<0.05. FTO, fat mass and obesity-associated protein; m^{6}A, N6-methyladenosine; SAKI, sepsis-induced acute kidney injury; HCs healthy controls; NC, negative control; IHC, immunohistochemistry; CLP, cecal ligation and puncture.

inflammatory factors indicated that FTO attenuated the activation of inflammatory pathways by inhibiting the activation of the NF-κB pathway (Figs. 2N and S1J). Next, western blot analysis of macrophage polarization markers, specifically CD86 and CD206, revealed that the upregulation of FTO led to a reduction in CD86 expression and an increase in CD206 expression (Fig. S1K and L). These findings suggested that M1 macrophage polarization is decreased by FTO, potentially representing a mechanism through which FTO attenuates the secretion of inflammatory factors. Overall, the overexpression of FTO reduced the LPS-induced inflammatory response.

Identification of MMP-9 as the key target of m^{6}A modification. To elucidate the underlying mechanism through which FTO exerts anti-inflammatory effects in SAKI, transcriptome sequencing (RNA-seq) and MeRIP-seq were utilized to investigate transcriptional alterations in macrophages stimulated with LPS (Fig. 3A). First, hierarchical clustering revealed 2169 upregulated genes and 1738 downregulated genes after LPS treatment (Fig. 3B). An earlier study demonstrated that FTO modulated the TNF-α-induced inflammatory response in cementoblasts through m^{6}A modification of MMP-9 (33). Specifically, consistent with the results of the analysis of patients with sepsis, FTO expression was decreased, whereas the expression levels of MMP-9, CXCL10 and IL-6 were upregulated in LPS-induced macrophages compared with control macrophages (Fig. 3C and D). Moreover, Gene Ontology (GO) analysis of the DEGs revealed significant enrichment of several key GO terms associated with the immune response (Fig. 3E), including the TNF-α signaling pathway and the IL-6/JAK/STAT3 pathway (P<0.05; Fig. 3F). When the m^{6}A methylomes of macrophages were mapped, the m^{6}A consensus sequence GGAC (RRACH) motif was highly enriched within m^{6}A sites in the immunopurified RNA (Fig. 3G). MMP-9 was identified as a candidate gene that markedly overlapped between the mRNA-seq data; it demonstrated a greater than 60-fold change (P<0.05) between the WT and LPS-stimulated macrophages, and the m^{6}A level on this gene was more than 16 times greater than that in the

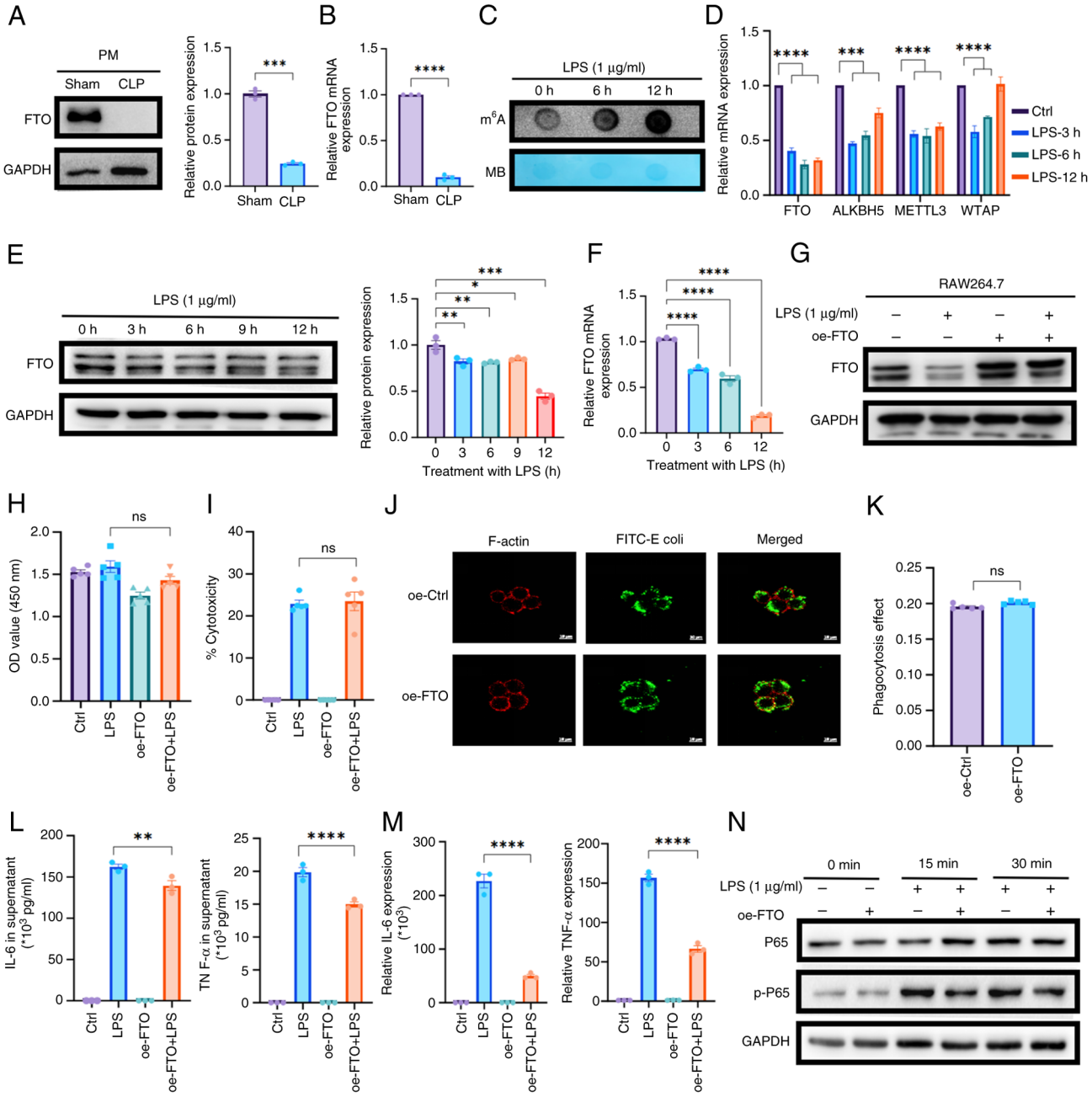

Figure 2. FTO modulates macrophage function and inflammatory responses in SAKI. (A) Western blotting and (B) qPCR revealed the downregulation of FTO expression in PMs isolated from septic mice compared with those from sham-operated controls (n=3). (C) Dot blot analysis revealed a time-dependent increase in m^{6}A methylation levels in RAW264.7 cells treated with LPS (1 μg/ml) for 0, 6 and 12 h. (D) qPCR analysis of m^{6}A-related enzymes in LPS-treated macrophages. (E) Western blotting and (F) qPCR demonstrated a time-dependent reduction in FTO protein expression in LPS-treated RAW264.7 cells. (G) Western blotting confirmed FTO overexpression in oe-FTO macrophages with or without treatment with LPS for 12 h. (H) CCK-8 and (I) LDH assays revealed that FTO overexpression does not induce cytotoxicity or affect macrophage proliferation. (J and K) Phagocytosis assays demonstrated that compared with control treatment, upregulation of FTO expression did not alter the phagocytic capacity of macrophages (original magnification, x63). (L) ELISA revealed that overexpression of FTO expression markedly inhibited the secretion of IL-6 and TNF-α. (M) qPCR experiments confirmed the suppressive effect of FTO on the mRNA expression levels of IL-6 and TNF-α. (N) Western blot analysis revealed that FTO attenuated the activation of inflammatory pathways by inhibiting NF-κB signaling. *P<0.05; **P<0.01; ***P<0.001; ****P<0.0001; ns, not significant. FTO, fat mass and obesity-associated protein; SAKI, sepsis-induced acute kidney injury; qPCR, quantitative PCR; PMs, peritoneal macrophages; LPS, lipopolysaccharide; m^{6}A, N6-methyladenosine; oe, over expression; LDH, lactate dehydrogenase; ELISA, enzyme-linked immunosorbent assay.

input (P<0.05). Different m^{6}A peaks were detected around the 3' untranslated region (UTR) of MMP-9 mRNA in macrophages (Fig. 3H). Additionally, transcriptomic sequencing was conducted to compare the gene expression profiles of macrophages with FTO overexpression after 6 h of LPS stimulation. mRNA-seq analysis revealed that the DEGs were markedly enriched in pathways related to the inflammatory response, such as cytokine-cytokine receptor interactions, highlighting their role in regulating proinflammatory signaling pathways (P<0.05; Fig. 3I). Specifically, elevated FTO levels are associated with increased MMP-9 expression, whereas increased FTO levels lead to markedly reduced IL-6 expression (Fig. 3J).

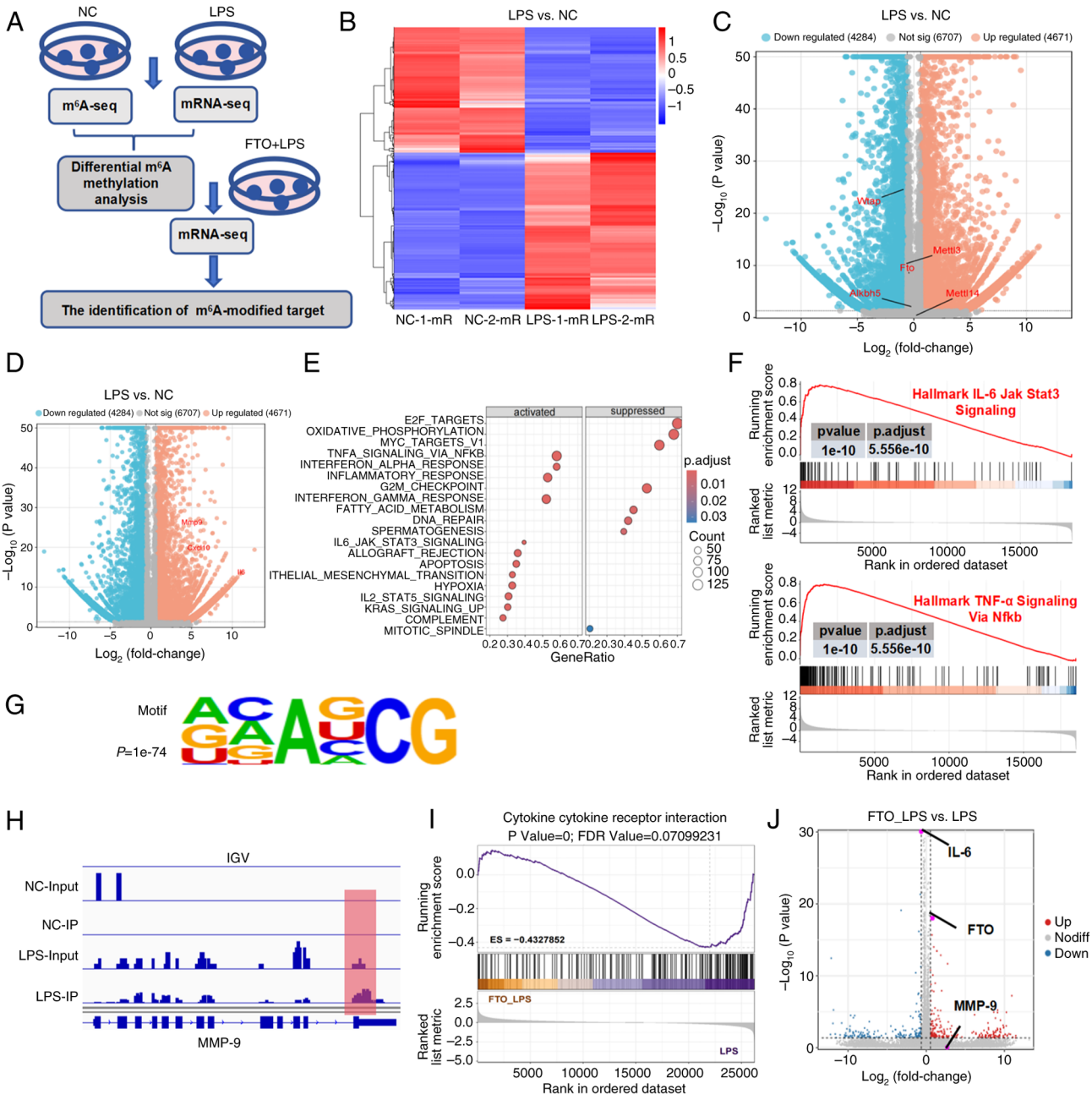

Figure 3. MMP-9 is the key target of FTO-mediated m^{6}A modification. (A) Flowchart of the multiomics analysis of macrophages. (B) Hierarchical clustering of differentially expressed genes in macrophages following LPS treatment. Volcano plot showing (C) downregulated FTO expression and (D) upregulated MMP-9 expression in LPS-induced macrophages compared with NC. (E) GO analysis of the DEGs revealed that the DEGs were enriched in immune response-related terms. (F) GSEA revealed that key pathways, including the TNF-α signaling and IL-6/JAK/STAT3 pathways, were markedly associated with the inflammatory response in LPS-treated macrophages. (G) Motif analysis of m^{6}A methylomes in macrophages. (H) Integrative Genomics Viewer image showing that the m^{6}A peaks of MMP-9 mRNA were near the 3'UTR. (I) mRNA-seq revealed that DEGs associated with FTO overexpression in LPS-stimulated macrophages were enriched in cytokine-cytokine receptor interaction pathways. (J) Volcano plot showing that elevated FTO levels were associated with increased MMP-9 expression. MMP-9, matrix metalloproteinase 9; FTO, fat mass and obesity-associated protein; m^{6}A, N6-methyladenosine; LPS, lipopolysaccharide; NC, negative control; GO, gene ontology; DEGs, differentially expressed genes; gene set enrichment analysis; TNF-α, tumor necrosis factor-α; IL-6, interleukin- 6.

FTO increases MMP-9 levels through m^{6}A modification. MMP-9 is the most extensively investigated MMP and is known for its critical involvement in numerous biological processes (34). To determine whether MMP-9 functions as a downstream target of FTO in macrophages, MeRIP-qPCR was conducted, which confirmed that m^{6}A-enriched MMP-9 mRNA levels were reduced by ~20-fold in oe-FTO macrophages treated with LPS (oe-FTO+LPS; Fig. 4A). Notably, compared with that in the respective LPS-treated group (LPS group), the MMP-9 expression levels in both bone marrow-derived macrophages (Fig. S1M and N) and RAW264.7 macrophages (Figs. 4B and C and S2A) markedly increased in response to overexpression with FTO. These findings were further corroborated by IF assays, which confirmed that elevated FTO levels led to the upregulation of MMP-9 in RAW264.7 cells (Fig. 4D). The present study further explored the potential mechanisms involved in the m^{6}A-regulated expression of MMP-9. The LPS and oe-FTO+LPS groups

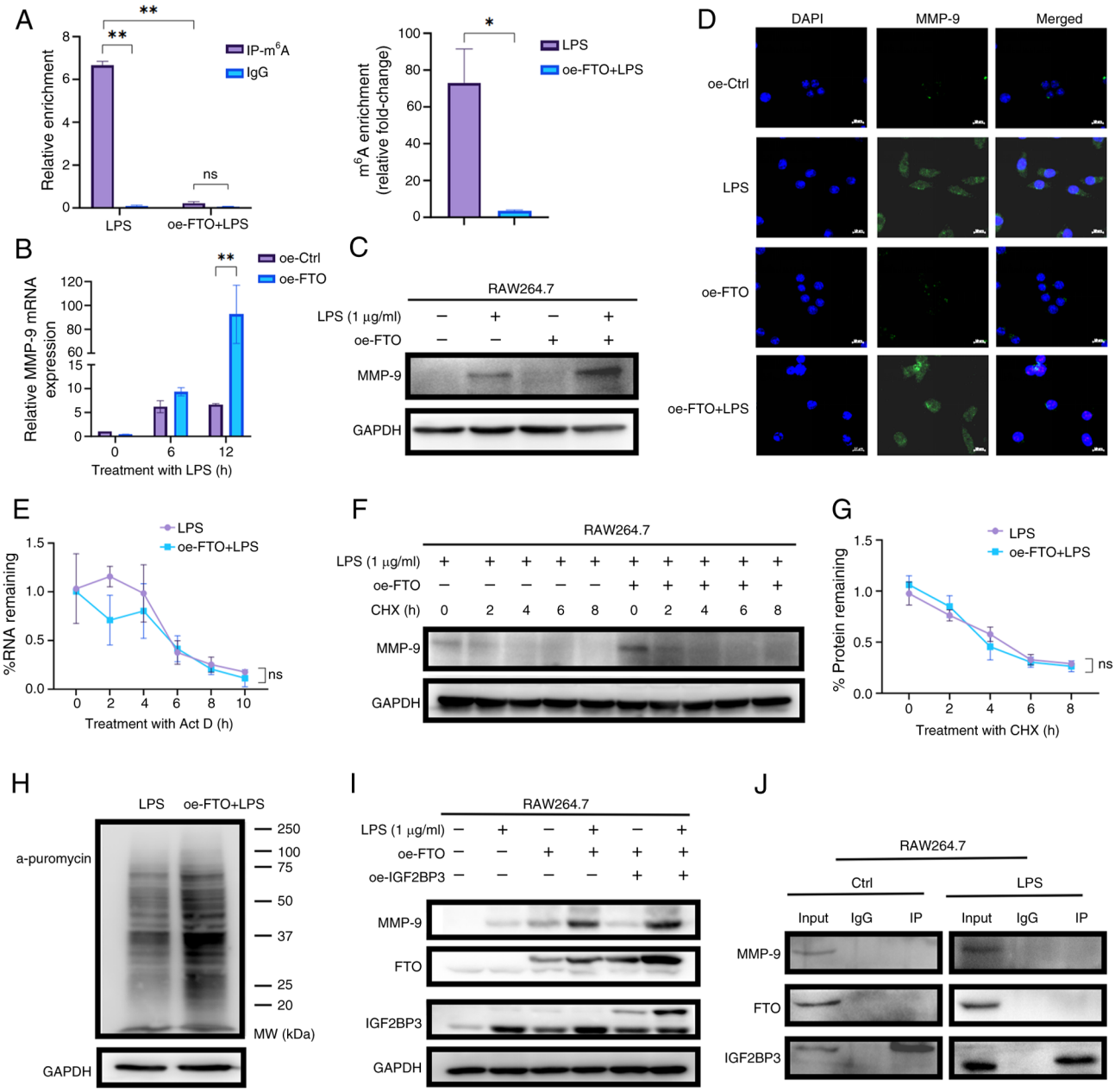

Figure 4. FTO upregulates MMP-9 expression in an m^{6}A-dependent manner in macrophages. (A) MeRIP-qPCR confirmed the decreased level of m^{6}A modification of MMP-9 mRNA in LPS-treated macrophages overexpressing FTO. (B) qPCR and (C) western blot analyses demonstrated that compared with control macrophage treatment, LPS stimulation increased MMP-9 expression in FTO-overexpressing macrophages. (D) Immunofluorescence assays confirmed that elevated FTO levels upregulated MMP-9 protein expression in macrophages following LPS treatment. (E) Actinomycin D treatment revealed that FTO-mediated m^{6}A modification did not markedly affect the mRNA stability of MMP-9 in macrophages treated with LPS for 12 h. (F) CHX treatment and (G) quantification demonstrated that FTO did not markedly affect MMP-9 protein stability following LPS treatment. (H) Puromycin labeling of nascent polypeptides revealed that FTO enhanced protein synthesis in macrophages treated with LPS for 12 h. (I) overexpression of IGF2BP3 in FTO-overexpressing macrophages led to the further upregulation of MMP-9. (J) Co-IP experiment identified the IGF2BP3 did not co-precipitate either with FTO or MMP9 in macrophages. *P<0.05; **P<0.01; ns, not significant. FTO, fat mass and obesity-associated protein; MMP-9, matrix metalloprot einase 9; m^{6}A, N6-methyladenosine; MeRIP-seq, methylated RNA immunoprecipitation sequencing; qPCR, quantitative PCR; LPS, lipopolysaccharide; oe, over expression; IGF2BP3, insulin-like growth factor 2 mRNA-binding protein 3.

were treated with Act-D to block transcription and the results suggested that FTO-mediated m^{6}A did not markedly affect the mRNA stability of MMP-9 in macrophages (Fig. 4E). Furthermore, the LPS and oe-FTO+LPS groups were treated with CHX to block protein translation and the data revealed that treatment with CHX attenuated FTO-induced MMP-9 upregulation, suggesting that FTO did not affect the protein stability of MMP-9 (Fig. 4F and G). A puromycin labeling assay revealed that FTO overexpression increased mRNA translation and drove an increase in nascent MMP-9 polypeptide synthesis following LPS treatment (Figs. 4H and S2B). Given that FTO-mediated m^{6}A demethylation enhances MMP-9 translation and considering the role of m^{6}A readers in modulating translational output, it was investigated whether the m^{6}A reader IGF2BP3 serves as a downstream amplifier. FTO-overexpressing (oe-FTO) RAW264.7 macrophages

were transduced with a lentiviral vector encoding IGF2BP3 (oe-IGF2BP3) or an empty control vector. The results revealed that FTO overexpression elevated both IGF2BP3 and MMP-9 levels and additional IGF2BP3 overexpression in FTO-overexpressing macrophages further amplified MMP-9 expression (Figs. 4I and S2C). To assess whether these proteins interact directly, Co-IP assays were performed in macrophages; however, IGF2BP3 did not co-precipitate either with FTO or MMP-9 (Fig. 4J). These results indicated that IGF2BP3 facilitated the upregulation of MMP-9 induced by FTO without directly binding with those two proteins. Thus, FTO-mediated m^{6}A demethylation enhances MMP-9 expression by promoting mRNA translation efficiency rather than increasing the stability of MMP-9 mRNA in macrophages in response to LPS.

MMP-9 deficiency exacerbates inflammatory responses in vitro and in vivo. In mice with SAKI, increased levels of MMP-9 were observed in the kidney (Figs. 5A and S2D), which aligns with the results obtained from CLP-derived PMs (Figs. 5B and C and S2F). Furthermore, the abundance of the MMP-9 protein substantially increased in a time-dependent manner in LPS-stimulated macrophages (Figs. 5D and S2G). Therefore, to investigate the functional role of MMP-9 in sepsis, MMP-9-knockdown macrophages (sh-MMP9) were established by transfecting them with lentiviral vectors encoding mouse MMP-9 shRNAs and their knockdown verified by western blotting (Fig. S2H). A CCK-8 assay was performed and it was found that MMP-9 knockdown did not affect macrophage proliferation (Fig. S2I). qPCR revealed that the knockdown of MMP-9 resulted in significant increases in the expression levels of IL-6 and TNF-α, whereas pretreatment with rMMP9 effectively reversed these effects (Fig. S2J). These findings were corroborated by the results of the ELISAs, which revealed that the depletion of MMP-9 strongly promoted the production of TNF-α and IL-6; however, pretreatment with recombinant MMP-9 effectively attenuated the increased release of TNF-α and IL-6 caused by MMP-9 knockdown (Fig. 5E). Additionally, MMP-9 was knocked down in FTO-overexpressing macrophages (FTO/MMP-9; Fig. S2K). Consistent with these findings, FTO upregulation impaired the proinflammatory effect on macrophages, whereas decreased MMP-9 reversed this effect, as demonstrated by qPCR and ELISAs (Fig. 5F-H). Moreover, western blot analysis revealed that MMP-9 depletion contributed to CD86 upregulation (Fig. S3A and B).

To further elucidate the role of MMP-9 in SAKI, *MMP9*$^{-/-}$ mice were subjected to CLP. The loss of MMP-9 through CRISPR-Cas editing consistently exacerbated kidney dysfunction 24 h post-CLP, as indicated by the elevated concentrations of BUN and Cr in the *MMP-9*$^{-/-}$ mice subjected to CLP (Fig. 5I). Furthermore, H&E staining revealed that the depletion of MMP-9 resulted in increased cytoplasmic vacuoles in the proximal tubule cells of the cortex and outer stripe of the outer medulla (OSOM) 24 h post-CLP compared with vacuoles in the WT group following CLP surgery (Fig. 5J and K). Moreover, qPCR analysis revealed that the deletion of MMP-9 increased the expression levels of IL-1β and IL-6 in the kidney (Fig. 5L). Since F4/80hi macrophages play a protective role in SAKI (35), an IHC assay was performed and it revealed that MMP-9 deficiency decreased the infiltration of F4/80+ macrophages in the kidney (Fig. 5M). Moreover, the IHC result revealed a slight increase in the expression of CD86 in *MMP9*$^{-/-}$ mice compared with that in WT controls after CLP surgery, which suggest that the proportion of CD86-positive macrophages is greater in *MMP9*$^{-/-}$ mice than in WT mice (Fig. S3C). These results indicated that the absence of MMP-9 exacerbated kidney damage and increased the levels of proinflammatory cytokines in CLP-treated mice.

FTO overexpression protects mice from CLP-induced SAKI. To elucidate the *in vivo* function of FTO, AAVs were used to induce the overexpression of FTO in murine models. The successful overexpression of FTO in the kidney was subsequently confirmed via IF and western blot analyses (Figs. 6A and Fig. S3D). Subsequent observations revealed a reduction in the sepsis mortality rate among the FTO-overexpressing mice subjected to CLP surgery (n=8; survival at 7 days: CLP+vector, 37.5%, vs. CLP+FTO-AAV, 87.5%; P<0.01; Fig. 6B). Moreover, H&E staining of pathological sections confirmed that FTO overexpression mitigated CLP-induced SAKI (Fig. 6C and D). FTO overexpression consistently alleviated kidney dysfunction 24 h post-CLP, as evidenced by low BUN levels in the CLP+FTO-AAV group (Fig. 6E). Moreover, ELISA revealed that the upregulation of FTO diminished the release of IL-6 and TNF-α (Fig. 6F). Furthermore, an IHC assay demonstrated that the abundance of MMP-9 increased in the kidneys of mice with SAKI and further increased with FTO overexpression (Fig. 6G). IF revealed that FTO overexpression also increased the infiltration of F4/80+ macrophages (Fig. 6A). Overall, these findings indicated that FTO-mediated MMP-9 upregulation modulates renal inflammation and increases the survival of CLP-treated mice.

Discussion

m^{6}A is a widespread posttranscriptional modification that induces epigenetic modifications in RNA. Mounting evidence has shown that m^{6}A modification profoundly affects the progression of various diseases, including metabolic syndrome, cancer and infectious diseases (36). However, the role of m^{6}A modification in kidney diseases, particularly SAKI remains relatively unexplored. FTO expression is closely involved in septic patients, showing a positive correlation with monocytes and exhibiting the highest diagnostic value among target genes, which gives it potential as a vital diagnostic biomarker for the treatment of SAKI (37). In the present study, consistent with analyses conducted on septic patients, *in vivo* experiments demonstrated that FTO expression is universally downregulated in key tissues and PMs when they are exposed to inflammatory stimuli. Furthermore, increased levels of the FTO protein were strongly associated with decreased m^{6}A modification and moderate inflammatory responses. Although both FTO and ALKBH5 were modestly downregulated in LPS-stimulated macrophages, FTO was prioritized for three converging reasons: (i) According to bioinformatics analysis and overall m^{6}A levels, the expression of FTO, which acts as a key eraser to induce m^{6}A demethylation, was markedly downregulated; (ii) the magnitude of FTO downregulation (mean 70%) upon LPS was more

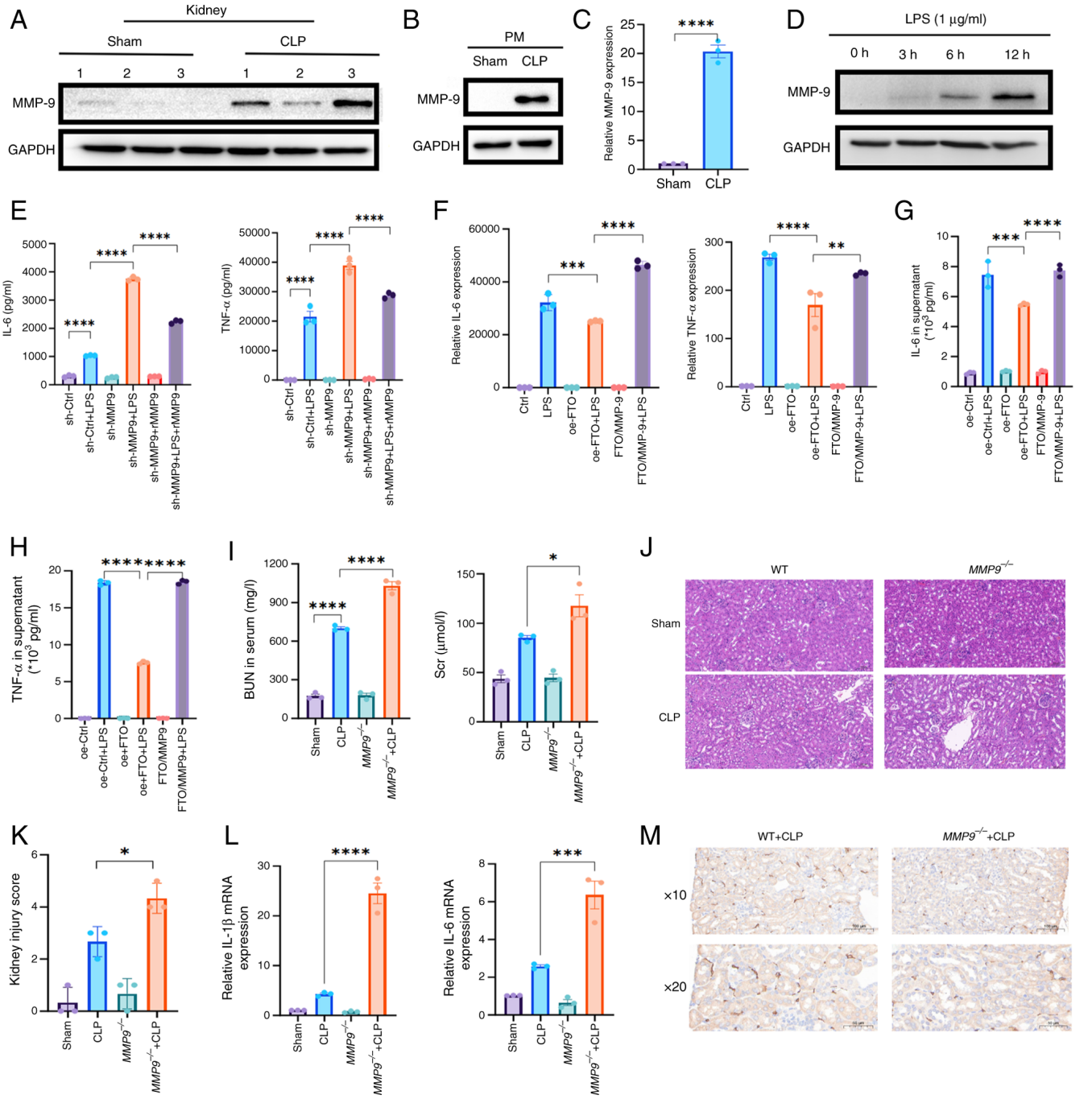

Figure 5. Depletion of MMP-9 increases the release of proinflammatory factors and exacerbated renal injury in SAKI model mice. (A) Western blot analysis revealed an increased abundance of MMP-9 in the kidneys of mice with SAKI (n=3). (B) Western blot and (C) qPCR analyses revealed an increased abundance of MMP-9 in CLP-derived PMs (n=3). (D) Western blot analysis revealed a time-dependent increase in the abundance of the MMP-9 protein in LPS-stimulated macrophages. (E) ELISA confirmed that MMP-9 depletion markedly increased the production of IL-6 and TNF-α. (F) qPCR analysis revealed markedly increased expression levels of IL-6 and TNF-α in MMP-9-depleted oe-FTO macrophages following LPS treatment. (G and H) ELISA confirmed that MMP-9 depletion markedly increased the production of TNF-α and IL-6 in MMP-9-depleted oe-FTO macrophages following LPS treatment. (I) The detection of BUN and Cr in the serum of *MMP9*$^{-/-}$ mice revealed that kidney dysfunction was exacerbated 24 h post-CLP (n=3). (J and K) H&E staining revealed more severe renal injury in *MMP9*$^{-/-}$ mice than in wild-type controls following CLP surgery (n=3, original magnification, x10). (L) qPCR analysis revealed that MMP-9 deletion increased the expression levels of IL-1β and IL-6 in the kidneys of CLP-treated mice (n=3). (M) IHC staining results showing the expression of F4/80 and reduced infiltration of F4/80+ macrophages in the kidneys of *MMP9*$^{-/-}$ mice after CLP surgery (n=3). *P<0.05; **P<0.01; ***P<0.001; ****P<0.0001. MMP-9, matrix metalloproteinase 9; SAKI, sepsis-induced acute kidney injury; qPCR, quantitative PCR; CLP, cecal ligation and puncture; PMs, peritoneal macrophages; LPS, lipopolysaccharide; ELISA, enzyme-linked immunosorbent assay; oe, over expression; BUN, blood urea nitrogen; Cr, creatinine; CLP, cecal ligation and puncture; H&E, hematoxylin and eosin; WT, wild-type.

pronounced than that of ALKH5 and consistent with the peak release of proinflammatory cytokines; (iii) This observation is corroborated by clinical data showing a significant reduction (~45%) of FTO expression in septic patients compared with healthy controls (38). Furthermore, a genome-wide association study reinforces the clinical relevance of the present study, reporting an association between lower FTO expression and an increased risk of AKI (39). While ALKBH5 may also

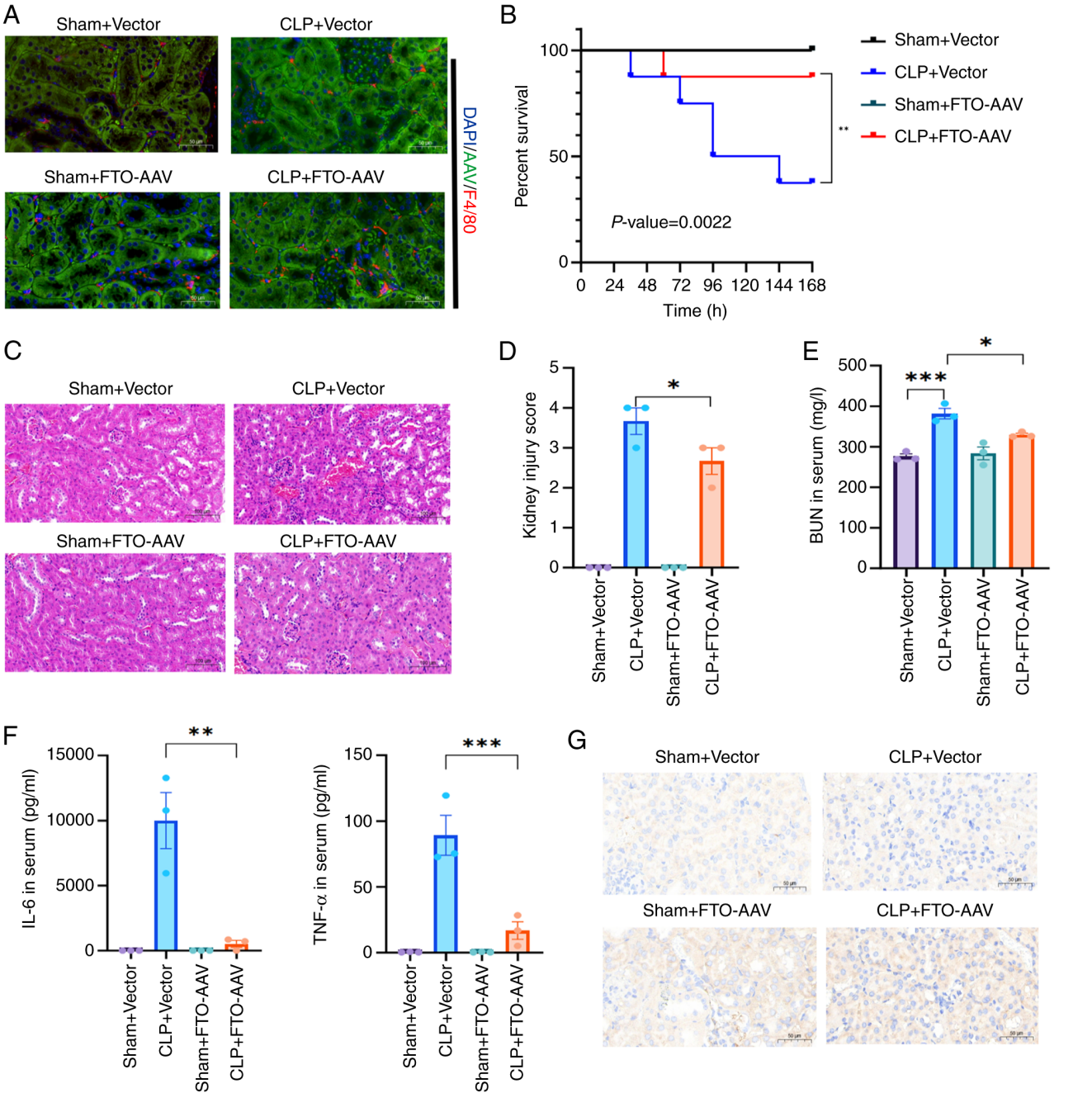

Figure 6. FTO overexpression ameliorated SAKI and improved survival in CLP mice. (A) Representative IF images showing successful overexpression of FTO in a murine model and the expression of F4/80 (n=3). (B) Survival curve using the log-rank test revealed a significant reduction in sepsis mortality in FTO-overexpressing mice compared with vector control mice (n=8; P=0.0022 <0.01). (C and D) H&E staining of kidney sections revealed that FTO overexpression mitigated CLP-induced renal injury (n=3). (E) Overexpression of FTO reduced the CLP-induced increase in serum BUN levels (n=3). (F) ELISAs revealed that FTO overexpression reduced serum IL-6 and TNF-α production (n=3). (G) An IHC assay revealed increased MMP-9 abundance in the kidneys of FTO-overexpressing mice after CLP surgery (n=3, original magnification, x20). *P<0.05 was considered to indicate statistical significance; **P<0.01; ***P<0.001. FTO, fat mass and obesity-associated protein; SAKI, sepsis-induced acute kidney injury; CLP, cecal ligation and puncture; IF, immunofluorescence; H&E, hematoxylin and eosin staining; BUN, blood urea nitrogen; ELISA, enzyme-linked immunosorbent assay; IHC, immunohistochemistry.

contribute, these observations provided a stronger, multi-level rationale for prioritizing FTO in the present study. The therapeutic potential of FTO was further underscored by the intervention study, wherein AAV-mediated FTO upregulation markedly prolonged the survival of CLP-treated mice, mitigated CLP-induced inflammation.

FTO is a member of the Fe(II) and 2-oxoglutarate-dependent dioxygenase family of proteins (40,41) and is associated with several other diseases, including Alzheimer's disease, neuropsychiatric disorders and various types of cancer (42,43). However, its role in inflammation appears to be context-dependent. For instance, FTO knockdown was reported to upregulate proinflammatory cytokines in rat cardiomyocytes (44), whereas ablation of FTO could inhibit NLRP3 inflammasome and ameliorate the inflammatory response in LPS-induced sepsis models (45). The present study found a distinct anti-inflammatory effect of FTO in sepsis-associated organ injury that may be attributed to its role in modulating MMP-9 expression

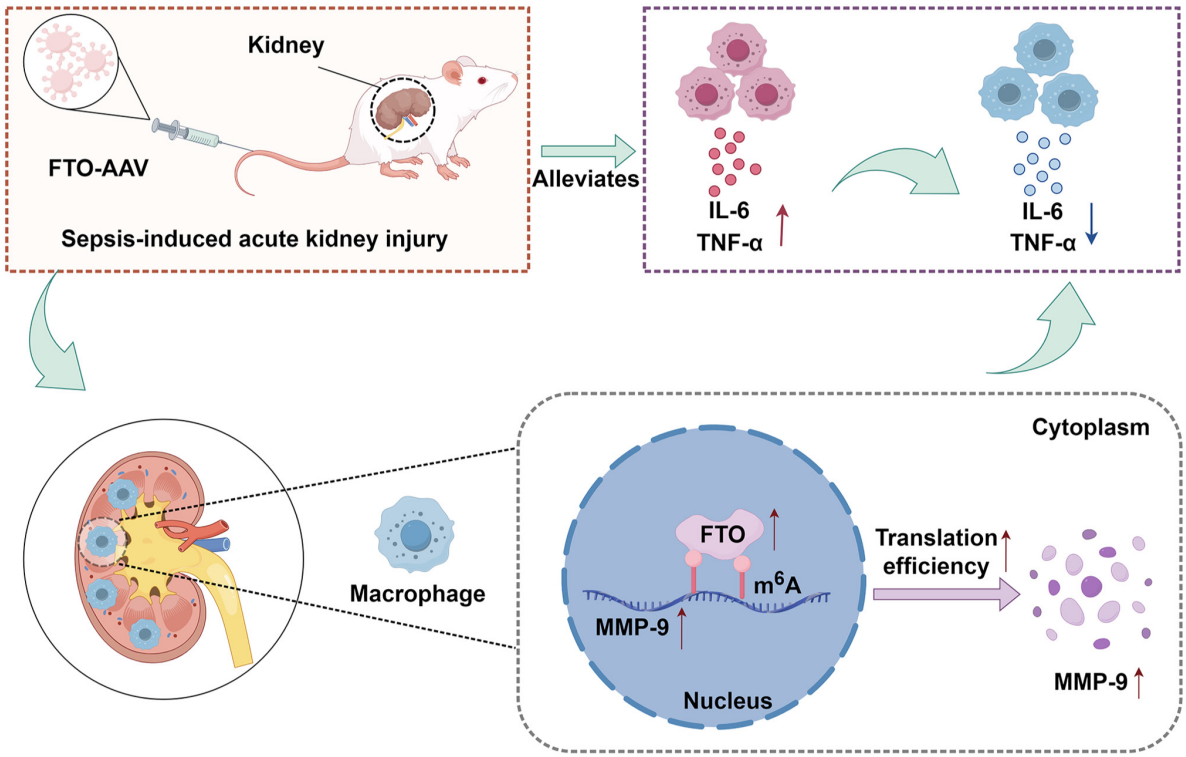

Figure 7. Graphical abstract generated by Figdraw 2.0 (https://www.figdraw.com/static/index.html#/) highlights the present study. FTO, fat mass and obesity-associated protein; AAV, adeno-associated virus; IL-6, interleukin-6; TNF-α, tumor necrosis factor-α; MMP-9, matrix metalloproteinase 9; m^{6}A, N6-methyladenosine.

and macrophage polarization towards an anti-inflammatory phenotype, which is distinct from the pro-inflammatory mechanisms observed in LPS-induced sepsis.

MMP-9 exhibits context-dependent functions across various cell types and disease etiologies of kidney injury, contributing to both physiological and pathological processes. For instance, MMP-9 deficiency increased the apoptosis of tubular epithelial cells and delay the recovery of renal function in folic acid induced AKI (46). MMP-9 also protected from glomerular tubule damage in cisplatin induced AKI (47). While in the model of ischemic AKI, MMP-9 deficiency mitigated microvascular loss which associated with renal hypoxia (48). The present study found that MMP-9 deficiency in macrophages increased IL-6 and TNF-α release and renal damage during SAKI, consisted with clinical observation that correlate low MMP-9 expression with worse survival (49). Mechanistically, MMP-9 was identified as a critical target of FTO-mediated m^{6}A modification in LPS-stimulated macrophages, with its expression being upregulated in response to FTO overexpression. Notably, elevated FTO primarily affects MMP-9 translation efficacy rather than mRNA stability, leading to increased MMP-9 levels in macrophages. However, the need for further investigation into the specific mechanisms by which FTO enhances MMP-9 mRNA translation efficiency remains a critical area for future research. The FTO/m^{6}A/MMP-9 protected against SAKI by suppressing inflammatory responses, which offers novel insights into therapeutic targets for SAKI (Fig. 7). Moreover, the clinical translatability of this axis is supported by studies reporting that decreased plasma MMP-9 and increased TIMP-1 in SAKI patients, with the MMP-9/TIMP-1 ratio being a superior prognostic indicator for disease severity and survival (50,51). Thus, it was hypothesized that the FTO/MMP-9 axis represents a promising biomarker candidate, worthy of future clinical validation to determine its prognostic and therapeutic utility.

Although recent studies have demonstrated certain therapeutic effects in animal models, the clinical application of FTO-AAV may encounter safety challenges, including potential immunogenicity and off-target effects. FTO is ubiquitously expressed and involved in critical physiological processes such as energy metabolism and insulin sensitivity (52,53). While the present study established a critical role of FTO in macrophage of SAKI, contributory or synergistic effects from FTO activity in other cell types cannot be excluded. Its overexpression in renal tubular epithelial cells, for example, has been shown to protect against ischemia-reperfusion injury by promoting autophagy (54). The current reliance on computational analyses and preclinical models thus represents another limitation for direct clinical translation.

The present study delineated a novel FTO/m^{6}A/MMP-9 signaling axis in macrophages that conferred protection against SAKI by modulating inflammatory responses. These findings provided new insights into the epigenetic mechanisms underlying SAKI and highlighted the therapeutic potential of targeting this pathway. In conclusion, a comprehensive understanding of the cell-specific actions of FTO and rigorous safety assessments are imperative before any therapeutic strategies can be advanced to the clinic.

Acknowledgements

Not applicable.

Funding

The present study was supported by projects from the Guangdong Basic and Applied Basic Research Foundation (grant no. 2025A1515011341), by the National Cancer Center/National Clinical Research Center for Cancer/Cancer Hospital & Shenzhen Hospital, the Chinese Academy of Medical Sciences and Peking Union Medical College, Shenzhen (grant nos. E010224010, SZ2020ZD012 and E010224009) and the Sanming Project of Medicine in Shenzhen (grant no. SZSM202311003).

Availability of data and materials

The data generated in the present study may be requested from the corresponding author.

Authors' contributions

ZC and QL provided scientific expertise, supervised the experiments and provided reagents. XC and ZC conceived and designed the study. XC, ZS and JZ performed the experiments, analyzed the data, and wrote the manuscript. JC and ZL collaboratively performed the animal experiments. ZY provided the scientific expertise and data for the animal experiments. ZC and QL confirm the authenticity of all the raw data. All authors read and approved the final manuscript.

Ethics approval and consent to participate

All animal experiments were approved by the Ethics Committee of Dongguan People's Hospital (approval no. IAC UC-AWEC-202406500R1).

Patient consent for publication

Not applicable.

Competing interests

The authors declare that they have no competing interests.

References

1. Gao Q, Zheng Y, Wang H, Hou L and Hu X: circSTRN3 aggravates sepsis-induced acute kidney injury by regulating miR-578/toll like receptor 4 axis. Bioengineered 13: 11388-11401, 2022.
2. Peerapornratana S, Manrique-Caballero CL, Gómez H and Kellum JA: Acute kidney injury from sepsis: Current concepts, epidemiology, pathophysiology, prevention and treatment. Kidney Int 96: 1083-1099, 2019.
3. He J, Zheng F, Qiu L, Wang Y, Zhang J, Ye H and Zhang Q: Plasma neutrophil extracellular traps in patients with sepsis-induced acute kidney injury serve as a new biomarker to predict 28-day survival outcomes of disease. Front Med (Lausanne) 11: 1496966, 2024.
4. Peng Y, Fang Y, Li Z, Liu C and Zhang W: Saa3 promotes pro-inflammatory macrophage differentiation and contributes to sepsis-induced AKI. Int Immunopharmacol 127: 111417, 2024.
5. Han HI, Skvarca LB, Espiritu EB, Davidson AJ and Hukriede NA: The role of macrophages during acute kidney injury: Destruction and repair. Pediatr Nephrol 34: 561-569, 2019.
6. He J, Zhao S and Duan M: The response of macrophages in sepsis-induced acute kidney injury. J Clin Med 12: 1101, 2023.
7. Karuppagounder V, Arumugam S, Thandavarayan RA, Sreedhar R, Giridharan VV, Afrin R, Harima M, Miyashita S, Hara M, Suzuki K, *et al*: Curcumin alleviates renal dysfunction and suppresses inflammation by shifting from M1 to M2 macrophage polarization in daunorubicin induced nephrotoxicity in rats. Cytokine 84: 1-9, 2016.
8. Huen SC and Cantley LG: Macrophage-mediated injury and repair after ischemic kidney injury. Pediatr Nephrol 30: 199-209, 2015.
9. Lee S, Huen S, Nishio H, Nishio S, Lee HK, Choi BS, Ruhrberg C and Cantley LG: Distinct macrophage phenotypes contribute to kidney injury and repair. J Am Soc Nephrol 22: 317-326, 2011.
10. Pérez S and Rius-Pérez S: Macrophage polarization and reprogramming in acute inflammation: A redox perspective. Antioxidants (Basel) 11: 1394, 2022.
11. Hu D, Wang Y, You Z, Lu Y and Liang C: lnc-MRGPRF-6:1 promotes M1 polarization of macrophage and inflammatory response through the TLR4-MyD88-MAPK pathway. Mediators Inflamm 2022: 6979117, 2022.
12. Zhu X, Tang H, Yang M and Yin K: N6-methyladenosine in macrophage function: A novel target for metabolic diseases. Trends Endocrinol Metab 34: 66-84, 2023.
13. Hari Gopal S, Alenghat T and Pammi M: Early life epigenetics and childhood outcomes: A scoping review. Pediatr Res 97: 1305-1314, 2025.
14. Harvey ZH, Chen Y and Jarosz DF: Protein-based inheritance: Epigenetics beyond the chromosome. Mol Cell 69: 195-202, 2018.
15. Zhang L, Lu Q and Chang C: Epigenetics in health and disease. Adv Exp Med Biol 1253: 3-55, 2020.
16. Liu Y, Yang D, Liu T, Chen J, Yu J and Yi P: N6-methyladenosine-mediated gene regulation and therapeutic implications. Trends Mol Med 29: 454-467, 2023.
17. Mao Y, Jiang F, Xu XJ, Zhou LB, Jin R, Zhuang LL, Juan CX and Zhou GP: Inhibition of IGF2BP1 attenuates renal injury and inflammation by alleviating m6A modifications and E2F1/MIF pathway. Int J Biol Sci 19: 593-609, 2023.
18. Zhao Y, Ding W, Cai Y, Li Q, Zhang W, Bai Y, Zhang Y, Xu Q and Feng Z: The m^6A eraser FTO suppresses ferroptosis via mediating ACSL4 in LPS-induced macrophage inflammation. Biochim Biophys Acta Mol Basis Dis 1870: 167354, 2024.
19. Cao F, Chen G, Xu Y, Wang X, Tang X, Zhang W, Song X, Yang X, Zeng W and Xie J: METTL14 contributes to acute lung injury by stabilizing NLRP3 expression in an IGF2BP2-dependent manner. Cell Death Dis 15: 43, 2024.
20. Dolinay T, Kim YS, Howrylak J, Hunninghake GM, An CH, Fredenburgh L, Massaro AF, Rogers A, Gazourian L, Nakahira K, *et al*: Inflammasome-regulated cytokines are critical mediators of acute lung injury. Am J Respir Crit Care Med 185: 1225-1234, 2012.
21. McGrath FM, Francis A, Fatovich DM, Macdonald SP, Arendts G, Woo AJ and Bosio E: Genes involved in platelet aggregation and activation are downregulated during acute anaphylaxis in humans. Clin Transl Immunology 11: e1435, 2022.
22. Yang H, Wang H, Shivalila CS, Cheng AW, Shi L and Jaenisch R: One-step generation of mice carrying reporter and conditional alleles by CRISPR/Cas-mediated genome engineering. CELL 154: 1370-1379, 2013.
23. Rittirsch D, Huber-Lang MS, Flierl MA and Ward PA: Immunodesign of experimental sepsis by cecal ligation and puncture. Nat Protoc 4: 31-36, 2009.
24. Liu Y, Song R, Zhao L, Lu Z, Li Y, Zhan X, Lu F, Yang J, Niu Y and Cao X: m^6A demethylase ALKBH5 is required for antibacterial innate defense by intrinsic motivation of neutrophil migration. Signal Transduct Target Ther 7: 194, 2022.
25. Aronoff GR, Sloan RS, Dinwiddie CJ Jr, Glant MD, Fineberg NS and Luft FC: Effects of vancomycin on renal function in rats. Antimicrob Agents Chemother 19: 306-308, 1981.
26. Chen Y, Wei W, Fu J, Zhang T, Zhao J and Ma T: Forsythiaside A ameliorates sepsis-induced acute kidney injury via anti-inflammation and antiapoptotic effects by regulating endoplasmic reticulum stress. BMC Complement Med Ther 23: 35, 2023.
27. Livak KJ and Schmittgen TD: Analysis of relative gene expression data using real-time quantitative PCR and the 2(-Delta Delta C(T)) method. Methods 25: 402-408, 2001.
28. Gallo-Oller G, Ordoñez R and Dotor J: A new background subtraction method for western blot densitometry band quantification through image analysis software. J Immunol Methods 457: 1-5, 2018.

29. Carson WF, Cavassani KA, Dou Y and Kunkel SL: Epigenetic regulation of immune cell functions during post-septic immunosuppression. Epigenetics 6: 273-283, 2011.
30. Córneo EDS, Michels M and Dal-Pizzol F: Sepsis, immunosuppression and the role of epigenetic mechanisms. Expert Rev Clin Immunol 17: 169-176, 2021.
31. Mu YF, Mao ZH, Pan SK, Liu DW, Liu ZS, Wu P and Gao ZX: Macrophage-driven inflammation in acute kidney injury: Therapeutic opportunities and challenges. Transl Res 278: 1-9, 2025.
32. Li T, Qu J, Hu C, Pang J, Qian Y, Li Y and Peng Z: Macrophage migration inhibitory factor (MIF) suppresses mitophagy through disturbing the protein interaction of PINK1-Parkin in sepsis-associated acute kidney injury. Cell Death Dis 15: 473, 2024.
33. Li B, Du M, Sun Q, Cao Z and He H: m^6 A demethylase Fto regulates the TNF-α-induced inflammatory response in cementoblasts. Oral Dis 29: 2806-2815, 2023.
34. Huang H: Matrix metalloproteinase-9 (MMP-9) as a cancer biomarker and MMP-9 biosensors: Recent advances. Sensors (Basel) 18: 3249, 2018.
35. Privratsky JR, Ide S, Chen Y, Kitai H, Ren J, Fradin H, Lu X, Souma T and Crowley SD: A macrophage-endothelial immunoregulatory axis ameliorates septic acute kidney injury. Kidney Int 103: 514-528, 2023.
36. Wiener D and Schwartz S: The epitranscriptome beyond m^{6}A. Nat Rev Genet 22: 119-131, 2021.
37. Zhang Q, Bao X, Cui M, Wang C, Ji J, Jing J, Zhou X, Chen K and Tang L: Identification and validation of key biomarkers based on RNA methylation genes in sepsis. Front Immunol 14: 1231898, 2023.
38. Zeng H, Xu J, Wu R, Wang X, Jiang Y, Wang Q, Guo J and Xiao F: FTO alleviated ferroptosis in septic cardiomyopathy via mediating the m6A modification of BACH1. Biochim Biophys Acta Mol Basis Dis 1870: 167307, 2024.
39. Siew ED, Hellwege JN, Hung AM, Birkelo BC, Vincz AJ, Parr SK, Denton J, Greevy RA, Robinson-Cohen C, Liu H, *et al*: Genome-wide association study of hospitalized patients and acute kidney injury. Kidney Int 106: 291-301, 2024.
40. Flamand MN, Tegowski M and Meyer KD: The proteins of mRNA modification: Writers, readers, and erasers. Annu Rev Biochem 92: 145-173, 2023.
41. Fedeles BI, Singh V, Delaney JC, Li D and Essigmann JM: The AlkB family of Fe(II)/α-Ketoglutarate-dependent dioxygenases: Repairing nucleic acid alkylation damage and beyond. J Biol Chem 290: 20734-20742, 2015.
42. Li Y, Su R, Deng X, Chen Y and Chen J: FTO in cancer: Functions, molecular mechanisms, and therapeutic implications. Trends Cancer 8: 598-614, 2022.
43. Reitz C, Tosto G, Mayeux R, Luchsinger JA NIA-LOAD/NCRAD Family Study Group and Alzheimer's Disease Neuroimaging Initiative: Genetic variants in the fat and obesity associated (FTO) gene and risk of Alzheimer's disease. PLoS One 7: e50354, 2012.
44. Dubey PK, Patil M, Singh S, Dubey S, Ahuja P, Verma SK and Krishnamurthy P: Increased m6A-RNA methylation and FTO suppression is associated with myocardial inflammation and dysfunction during endotoxemia in mice. Mol Cell Biochem 477: 129-141, 2022.
45. Luo J, Wang F, Sun F, Yue T, Zhou Q, Yang C, Rong S, Yang P, Xiong F, Yu Q, *et al*: Targeted inhibition of FTO demethylase protects mice against LPS-induced septic shock by suppressing NLRP3 inflammasome. Front Immunol 12: 663295, 2021.
46. Bengatta S, Arnould C, Letavernier E, Monge M, de Préneuf HM, Werb Z, Ronco P and Lelongt B: MMP9 and SCF protect from apoptosis in acute kidney injury. J Am Soc Nephrol 20: 787-797, 2009.
47. Liu J, Li Z, Lao Y, Jin X, Wang Y, Jiang B, He R and Yang S: Network pharmacology, molecular docking, and experimental verification reveal the mechanism of San-Huang decoction in treating acute kidney injury. Front Pharmacol 14: 1060464, 2023.
48. Lee SY, Hörbelt M, Mang HE, Knipe NL, Bacallao RL, Sado Y and Sutton TA: MMP-9 gene deletion mitigates microvascular loss in a model of ischemic acute kidney injury. Am J Physiol Renal Physiol 301: F101-F109, 2011.
49. Fiotti N, Mearelli F, Di Girolamo FG, Castello LM, Nunnari A, Di Somma S, Lupia E, Colonetti E, Muiesan ML, Montrucchio G, *et al*: Genetic variants of matrix metalloproteinase and sepsis: The need speed study. Biomolecules 12: 279, 2022.
50. Maitra SR, Jacob A, Zhou M and Wang P: Modulation of matrix metalloproteinase-9 and tissue inhibitor of matrix metalloproteinase-1 in sepsis. Int J Clin Exp Med 3: 180-185, 2010.
51. Niño ME, Serrano SE, Niño DC, McCosham DM, Cardenas ME, Villareal VP, Lopez M, Pazin-Filho A, Jaimes FA, Cunha F, *et al*: TIMP1 and MMP9 are predictors of mortality in septic patients in the emergency department and intensive care unit unlike MMP9/TIMP1 ratio: Multivariate model. PLoS One 12: e171191, 2017.
52. Mizuno TM: Fat mass and obesity associated (FTO) gene and hepatic glucose and lipid metabolism. Nutrients 10: 1600, 2018.
53. Benak D, Sevcikova A, Holzerova K and Hlavackova M: FTO in health and disease. Front Cell Dev Biol 12: 1500394, 2024.
54. Zhang C, Guan G, Wang J, Wei H and Cai J: MicroRNA-192-5p downregulates fat mass and obesity-associated protein to aggravate renal ischemia/reperfusion injury. Ren Fail 45: 2285869, 2023.